論文 / 著書情報
Article / Book Information

Title	Seismic Performance and Evaluation of Controlled Spine Frames Applied in High-rise Buildings
Authors	Xingchen Chen, Toru Takeuchi, Ryota Matsui
Citation	Earthquake Spectra
DOI	http://dx.doi.org/10.1193/080817EQS157M

EARTHQUAKE SPECTRA

The Professional Journal of the Earthquake Engineering Research Institute

PREPRINT

This preprint is a PDF of a manuscript that has been accepted for publication in *Earthquake Spectra*. It is the final version that was uploaded and approved by the author(s). While the paper has been through the usual rigorous peer review process for the Journal, it has not been copyedited, nor have the figures and tables been modified for final publication. Please also note that the paper may refer to online Appendices that are not yet available.

We have posted this preliminary version of the manuscript online in the interest of making the scientific findings available for distribution and citation as quickly as possible following acceptance. However, readers should be aware that the final, published version will look different from this version and may also have some differences in content.

The DOI for this manuscript and the correct format for citing the paper are given at the top of the online (html) abstract.

Once the final, published version of this paper is posted online, it will replace the preliminary version at the specified DOI.

Seismic Performance and Evaluation of Controlled Spine Frames Applied in High-rise Buildings

Xingchen Chen [a] , Toru Takeuchi [b] and Ryota Matsui [b]

A controlled spine frame system consists of moment frames and spine frames with concentrated energy-dissipating members. This system could guarantee the continuous usability of buildings against Japanese Level-2 (similar to DBE in California, U.S.) earthquake events, and the authors confirmed its excellent performance for preventing damage concentration in low-rise buildings. This study further investigates the effect of diverse structural properties on the seismic performance of controlled spine frames applied in high-rise buildings. The effect of building height, yield drift of dampers, spine-to-moment frame stiffness ratio, and damper-to-moment frame stiffness ratio are illustrated in detail and their optimal values are discussed. Besides, a segmented spine frame system is proposed for high-rise buildings. The simple evaluation procedure proposed by the authors for low-rise buildings, based on equivalent linearization techniques and response spectrum analyses, was modified to include higher-modes effects for high-rise buildings based on modal analysis. The modified evaluation method was verified by modal pushover and time-history analyses.

INTRODUCTION

Damage concentration in limited levels of frame structures has often occurred during past major earthquake events, which has raised attention for the need of improving their structural integrity. Various solutions were provided by previous researchers, such as the "strong-column weak-beam" concept, and the shear wall-frame dual system. Walls usually ensure better structural integrity because of their considerable stiffness. However, they may significantly increase the resisting force and input earthquake energy owing to period shift, and extensive damage may occur at the bottom levels of the shear walls, which is costly and time consuming to repair. In their study about the effect of foundation flexibility on the seismic performance of

[a] Former Graduate Student, Tokyo Institute of Technology, (Currently Hiroshima University, Hiroshima, Japan 739-8527)
[b] Department of Architecture and Building Engineering, Tokyo Institute of Technology, Tokyo, Japan 152-8550

a wall-frame system, Paulay and Priestley found that the loss of wall base restraint would not significantly impair the seismic performance of wall-frame systems. (T. Paulay et al. 1992) The beneficial spine effect of pin-based walls or columns on the seismic performance of wall-frame systems was verified by studies based on theoretical analyses of multi-degree-of-freedom models or dynamic analyses of building models up to 20 stories. (H. Akiyama et al. 1984; G. A. MacRae et al. 2004; B. Alavi et al. 2004; A. Tanimura et al. 1996) In recent years, various spine systems with energy-dissipating members were proposed for both new building applications and retrofitting. Qu et al. employed a pivoting spine concept in the seismic retrofitting of a concrete building in Japan. (Z. Qu et al. 2012) Janhunen et al. proposed a seismic retrofit solution by adding a single pivoting concrete spine to the core of a 14-story building to improve its drift pattern and to distribute yielding at all levels of the building. (B. Janhunen 2013) Eatherton et al. carried out a shake table test of an uplifting steel rocking frame system with post-tensioned (PT) strands to provide self-centering and proposed several design concepts for this system. (M. Eartherton et al. 2010, 2014) MacRae et al. concluded design considerations for rocking structures (G. MacRae et al. 2013). Djojo et al. proposed a rocking steel panel shear wall with energy dissipation devices (G. S. Djojo et al. 2014). Mahin et al. examined the Strongback system, which combines aspects of a traditional concentric braced frame with a stiff mast to prevent the tendency of damage concentration in a single or a few stories. (J. Lai et al. 2014) However, previous research mainly focused on the 1st-mode response that dominates building structures and there are few research results about the seismic performance of high-rise buildings adopting the moment frame with spine frame dual systems.

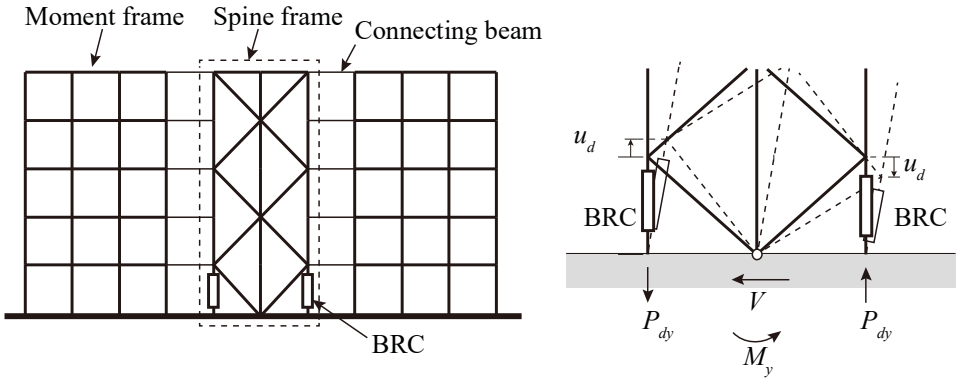

Figure 1. Concept of a controlled spine frame structure

A new controlled spine frame was proposed by the authors (T. Takeuchi et al. 2015; X. Chen et al. 2017), as shown in Fig. 1, and it was applied in the design of a new five-story research center at the Tokyo Tech's Suzukakedai campus. This spine frame consists of (1) a

stiff braced steel frame or reinforced concrete (RC) wall (i.e., the spine frame), (2) replaceable energy-dissipating members (herein called buckling restrained columns, BRC), and (3) envelope moment-resisting frames. The envelope moment frames are designed to remain elastic and to control the residual drifts, providing the self-centering force without resorting to post-tensioning. The input seismic energy is absorbed by the BRCs, which feature significant cumulative deformation capacity, and if required can easily be replaced following a large earthquake. This combination of structural elements effectively reduces the repair cost and downtime of buildings after suffering major earthquakes.

The authors verified the excellent performance of low-rise buildings adopting the proposed spine frame system in preventing damage concentration in weak stories, and their sufficient self-centering capacity against large earthquake events. The relation between seismic performance and key structural parameters was studied. A simple yet very applicable design method was established with clear limitations and recommendations.

However, it was found in the previous study that the simple controlled spine system is less sufficient for high-rise buildings because of the higher vibration modes, and larger flexural deformation of the spine frame caused by higher bending moment. Also the proposed simplified response evaluation method using the assumption of first-mode dominant response showed large error for higher structures. In this study, various segmented spine systems are proposed to overcome the limitation of height, and their effects are compared with the simple spine frame. Moreover, two simple response evaluation methods are applied. One is the modal pushover analysis, and another is modified response spectrum method considering higher vibration modes. The procedures of each method are proposed and the validity of them is confirmed.

BENCHMARK BUILDINGS OF THE CONTROLLED SPINE FRAMES

BENCHMARK BUILDINGS

A parametric study based on a nonlinear time-history analysis was used to investigate the seismic performance of the controlled spine system with diverse structural properties. The benchmark structures utilized in this study represent typical steel-structure office buildings, as shown in Figs. 2(a) to (c). Besides the continuous single spine (Cnt) model, the corresponding shear wall (SW) model was compared with the Cnt model in the cases of 5-, 10-, 20-, and 30-story buildings. In order to reduce the base shear of high-rise buildings utilizing the controlled

spine frame system, besides the continuous spine, the authors investigated alternative spine configurations, in particular the segmented spine frame configurations illustrated in Fig. 2(d). In segmented spine frame (Sgt) structures, there are two or three spine frames arranged in series along the height of these structures. All of them are pin-connected at the bottom center to the lower spine or to the foundation structures, and equipped with BRCs at both edges.

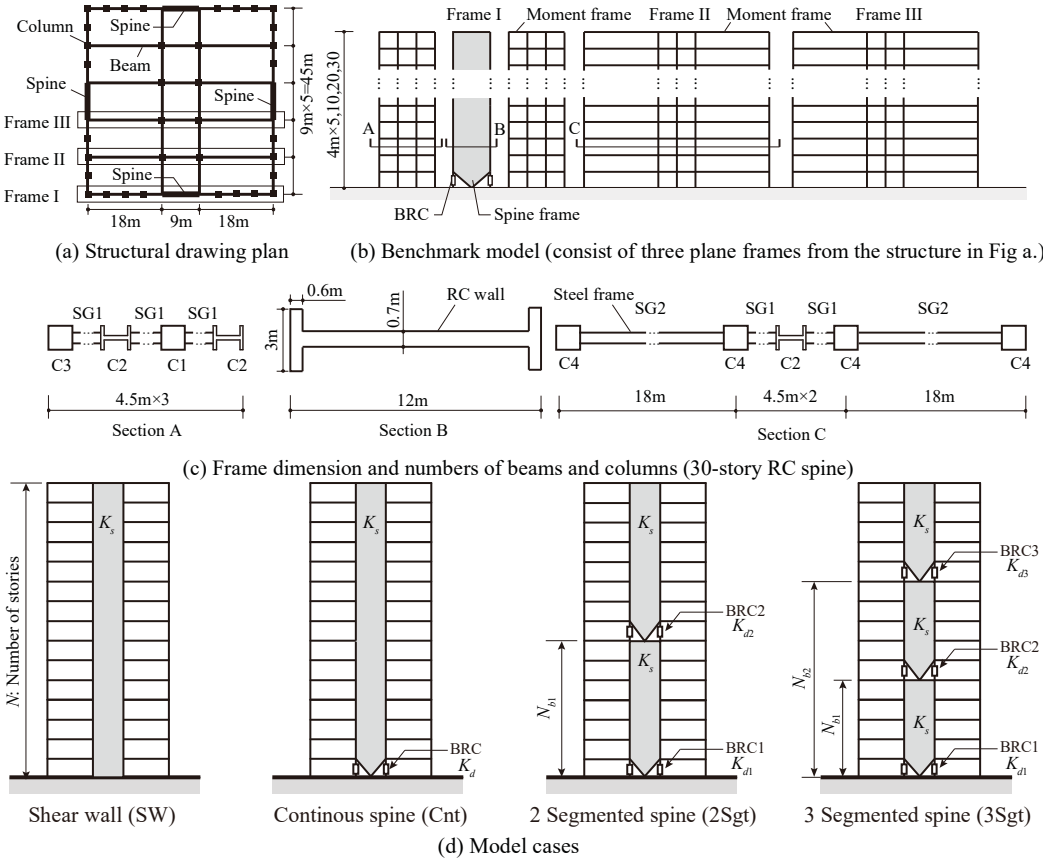

Figure 2. Benchmark models of the controlled spine frame structures

The two-segment-spine (Sgt2) and three-segment-spine (Sgt3) models were compared with the Cnt model in the cases of 20- and 30-story buildings, as shown in Fig. 2(d). The four different height Cnt structures were designed in elastic ranges as per the base shear ratio (base shear normalized by seismic weight of the structure) of 0.03–0.15. The moment frames and spine frames were assumed to remain elastic during Japanese Level-2 (similar to DBE in California, U.S.) earthquake events. Although the spine frames can suppress the soft story formation, for this study the lateral stiffness of the moment frames was set approximately proportional to the story shear. The spine frames in the 5- and 10-story buildings are assumed

to be pin-supported steel trusses, and those in the 20- and 30-story buildings are pin-supported RC walls, to achieve the required stiffness for the parameter studies. The RC walls are assumed to be pre-stressed by post-tensioning tendons to prevent cracking, and thus, stiffness degradation of the RC wall is not considered. The regular member dimensions in each benchmark model are summarized in Table 1.

Table 1 (a). Dimensions of beams and columns in the moment frame (unit: mm)

Models	C1	C2	C3	C4	SG1	SG2
5-story	□-500×19-22	H-500×350×25×28-32	□-500×19-22	□-600×32	H-600×300×12×22-25	H-1000×300×19×32
10-story	□-600×19-28	H-650×400×16×22-28	□-600×19-25	□-650×28-32	H-650×300×16×25-32	H-900×300×19×25
20-story	□-600×19-28	H-650×400×16×22-28	□-600×19-25	□-650×28-32	H-700×300×16×22-30	H-900×300×19×25
30-story	□-700×19-28	H-750×500×16×22-28	□-700×19-25	□-750×28-32	H-750×300×16×22-32	H-1000×300×19×25

Table 1 (b). Structural properties of spine frame, BRC hinge[*1], and equivalent stiffnesses[*2]

Models	Spine frame		BRC hinge		Equivalent stiffness		
	EI (kNm^2)	GA (kN)	M_y (kNm)	θ_y (rad)	K_f (kN/m)	K_s (kN/m)	K_d (kN/m)
5-story	2.9×10^8	4.0×10^6	3.0×10^4	0.10%	1.4×10^5	7.0×10^4	1.4×10^5
10-story	9.1×10^8	1.2×10^7	6.4×10^4	0.10%	7.5×10^4	3.8×10^4	7.5×10^4
20-story	2.0×10^9	1.4×10^8	1.3×10^5	0.10%	3.9×10^4	1.2×10^4	3.9×10^4
30-story	6.0×10^9	2.1×10^8	2.6×10^5	0.10%	3.5×10^4	1.0×10^4	3.5×10^4

*1 BRC hinge represents a pair of BRCs at the bottom or segment level of the spine frame: $M_y = F_{BRC\_y}\cdot b$, $\theta_y = 2u_{BRC\_y}/b$, where F_{BRC_y} and u_{BRC_y} are the axial yielding force and deformation of a BRC, b is the lateral distance between a pair of BRCs.

*2 Equivalent stiffnesses are defined in Section 2.3

Member-by-member (MBM) models of the benchmark buildings were built in OpenSees. (http://opensees.berkeley.edu) Centerline dimension models, which ignore the effects of panel zones and gusset plates, were employed for all models. Beams, columns and braces or walls were modeled by displacement-based beam elements with elastic materials. P-Delta effects were not included. A rigid floor was assumed, to ensure that the rocking frame worked together with the envelope frame. In the modeling of BRCs, we adopted equivalent elastic modulus and equivalent strain hardening ratio in order to consider that contribution of the higher axial stiffness of the elastic portions of the same member. The material of BRCs were assumed to

have bilinear stress–strain relations with a kinematic hardening rule. Rayleigh damping with 0.02 critical damping ratio matching at the first and third modes was implemented in the model.

PARAMETERIZING OF KEY STRUCTURAL PROPERTIES

The key structural properties, which are considered highly related to the seismic performance of spine frame structures, are the stiffnesses of the moment frames, spine frames, and dampers. The stiffness of the moment frame, denoted by K_f, is given by Eq. (1)

$$K_f = \frac{12}{h^2 \sum_{n=1}^{N} \left(\frac{1}{(EI/h)_{cn}} + \frac{1}{(EI/l)_{bn}} \right)} \tag{1}$$

where h represents the story height; and $(EI/h)_{cn}$ and $(EI/l)_{bn}$ are the sums of line stiffness of all the columns and beams at the n-th story, respectively. N is the total number of stories.

The lateral stiffness of the spine frame, denoted by K_s, is defined in Eq. (2) considering both bending and shear stiffness.

$$K_{sb} = \frac{3(EI)_s}{H^3},\ K_{ss} = \frac{(GA)_s}{H},\ K_s = \frac{1}{\frac{1}{K_{ss}} + \frac{1}{K_{sb}}} \tag{2}$$

where $(EI)_s$ is the equivalent sectional bending stiffness of the spine frame; $(GA)_s$ is the equivalent sectional shear stiffness of the spine frame; H is the total height of the structure, which is identical to the height of the spine frame; and K_{sb} and K_{ss} are the equivalent bending stiffness and shear stiffness of the spine frame, respectively. The lateral stiffness of the dampers, denoted by K_d is calculated by Eq. (3)

$$K_d = \frac{F_{BRC\_y}(b)^2}{2u_{BRC\_y}(H_{eq})^2} \tag{3}$$

where u_{BRC_y} is the yield deformation of each BRC, b is the width of the spine frame, F_{BRC_y} represents the yielding force of the BRC, and H_{eq} is the equivalent height of the first mode. The representative stiffnesses are further parameterized into normalized stiffness ratios, which are the stiffness ratio of spine frame to moment frames, denoted by K_s/K_f, and the stiffness ratio of dampers to moment frames, denoted by K_d/K_f. They are used as the control parameters in

149 the parametric study. In the benchmark models, θ_y=0.1%, K_d/K_f=1.0, and K_s/K_f=0.5 in the 5-
150 and 10-story buildings, while K_s/K_f=0.3 in the 20- and 30-story buildings. Considering the
151 seismic design code and construction requirement, in the parametric study, K_d/K_f ranges from
152 0.5 to 4.0, and K_s/K_f ranges from 0.1 to 2.0. Table 2 summarizes the variables of the four
153 buildings, and a total of 564 cases were studied.

154 **Table 2.** Variables in the parametric study

Sgt3-**Ksf**0.3-**Nb**10-20-**Kdf**1.0-1.0-1.0
① ② ③ ④

① Model type
SW: Shear wall **Cnt**: Continous spine
Sgt2: 2 Segmented spines **Sgt3**: 3 Segmented spines

② Stiffness ratio of the spine and the moment frame
Ksf K_s/K_f

③ Stories of the upper BRCs
(excluded in SW or Cnt model)
Sgt2: **Nb** N_{b1}
Sgt3: **Nb** N_{b1}-N_{b2}

④ Stiffness ratio of the dampers and
the moment frame (excluded in SW model)
Cnt: **Kdf** K_d/K_f
Sgt2: **Kdf** K_{d1}/K_f-K_{d2}/K_f
Sgt3: **Kdf** K_{d1}/K_f-K_{d2}/K_f-K_{d3}/K_f

All	K_s/K_f	0.1	0.3	0.5	0.7	1	2			
Cnt	K_d/K_f	0	0.5	0.8	1	1.3	1.5	2	3	4
Sgt2	N_{b1}	3~29								
	K_{d1}/K_f	0	0.5	0.8	1	1.3	1.5			
	K_{d2}/K_{d1}	0.5	0.8	1						
Sgt3	N_{b1}	10~20								
	N_{b2}	14~28								
	$K_{d1(2,3)}/K_f$	1								

155

156 **INPUT GROUNDMOTIONS→TIME-HISTORY ANALYSES**

157 A time-history analysis was carried out to examine their seismic performance. The ground
158 motions used for the time history analysis include the artificial wave BCJ-L2 with duration of
159 120 s, as well as the observed waves El Centro NS (1940), JMA Kobe NS (1995), TAFT EW
160 (1925), and Hachinohe NS (1968), each of them 30 s long. The acceleration response spectra
161 of the four recorded ground motions were spectrally matched to follow the Japanese life-safety
162 design spectrum (BRI-L2), as shown in Fig. 3.

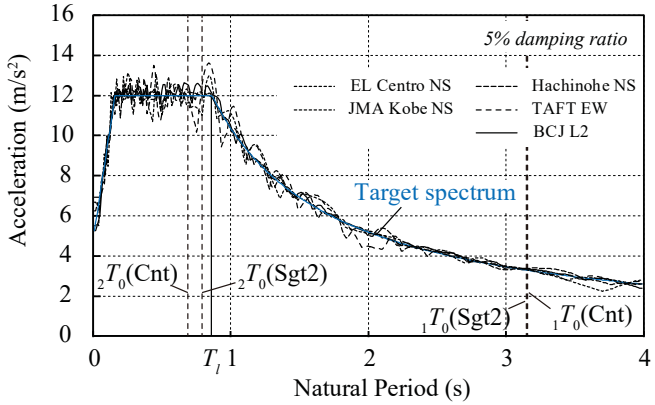

163
164 **Figure 3**. Acceleration spectra of normalized input ground motions

SEISMIC EVALUATION BASED ON MODAL PUSHOVER ANALYSIS

EVALUATION PROCEDURE

Besides the evaluations by time-history analyses using MBM models, two simplified response evaluation methods using the key parameters are proposed in the following. The modal pushover analysis (MPA) based on the structural dynamics theory has been commonly used for seismic evaluation (H. Krawinkler et al. 1998). In a typical MPA procedure, a suit of monotonically increasing lateral forces with an invariant height-wise distribution is loaded on the structure till a target deformation is reached (A. K. Chopra et al. 2002). Both the force distribution and target deformation are calculated by assuming that one mode response is predominant and the mode shape remains unchanged after the yielding mechanism occurs. The invariant force distribution cannot consider the redistribution of inertia forces after the yielding mechanism occurs, but they are conceptually and computationally simple for engineering practice. In the current study, a MPA procedure with invariant force distribution considering the contribution of higher modes is utilized for evaluating the proposed continuous and segmented spine frame structures applied in high-rise buildings, as shown in Fig. 4.

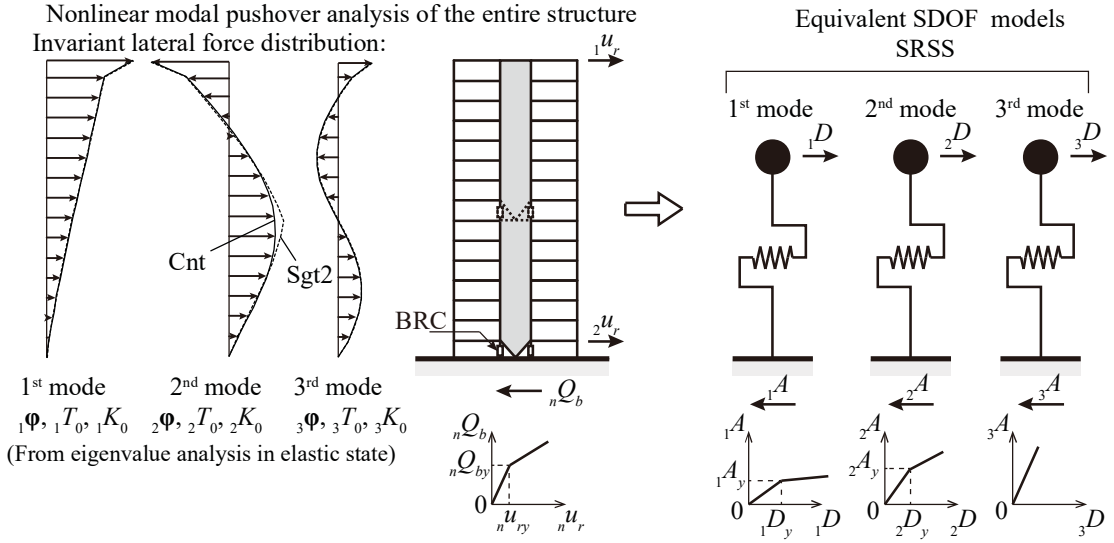

Figure 4. Nonlinear modal pushover analysis for spine frame structures

Chopra et al. proposed a modified MPA procedure assuming the higher modes as elastic, and verified its accuracy for regular frames. (A. K. Chopra et al. 2004) However, this assumption significantly overestimates the seismic performance, particularly the force response of spine frames in controlled spine frame structures. Therefore, a nonlinear pushover analysis is required for higher modes, at least for the second mode of spine frame structures.

The evaluation procedure is as follows:

Step 1. Compute the natural periods, ${}_nT_0$, and modes, ${}_n\boldsymbol{\varphi}$, for a linearly elastic vibration of the building.

Step 2. For the *n*th mode, develop the base shear-floor displacement, ${}_nQ_b - {}_nu_r$ pushover curve by nonlinear static analysis of the building using the lateral force distribution, ${}_n\mathbf{q}^*$ (Eq. (4)). (**m** is mass matrix)

$$ {}_n\mathbf{q}^* = \mathbf{m}\ {}_n\boldsymbol{\varphi} \tag{4}$$

Step 3. Convert the ${}_nQ_b - {}_nu_r$ pushover curve to the force-deformation, ${}_nA - {}_nD$, relation for the *n*-th mode inelastic SDOF system by utilizing Eq. (5) (${}_nM_{eq}$ is the effective modal mass. ${}_n\beta$ is called a modal participation factor. ${}_nu_r$ is reference floor displacement. ${}_nQ_b$ is base shear force.) Section "REFERENCE FLOOR" explains how to determine the reference floor.

$$ {}_nA = \frac{{}_nQ_b}{{}_nM_{eq}} \qquad {}_nD = \frac{{}_nu_r}{{}_n\beta\ {}_n\varphi_r},\ {}_n\beta = \frac{{}_n\boldsymbol{\varphi}^T\mathbf{m}\{1\}}{{}_n\boldsymbol{\varphi}^T\mathbf{m}\ {}_n\boldsymbol{\varphi}},\ {}_nM_{eq} = \frac{\left({}_n\boldsymbol{\varphi}^T\mathbf{m}\{1\}\right)^2}{{}_n\boldsymbol{\varphi}^T\mathbf{m}\ {}_n\boldsymbol{\varphi}} \tag{5}$$

Step 4. From ${}_nA - {}_nD$ relation determine the initial stiffness and hardening stiffness of the SDOF system.

Step 5. Evaluate the peak deformation ${}_nD$ by utilizing Eqs. (6)–(9) iteratively.

$$ {}_nh_{eq} = {}_nh_0 + \frac{2}{\pi\mu p}\ln\frac{\left(1-p+p\mu\right)}{\left(\mu\right)^p} \tag{6}$$

$$ {}_nT_{eq} = {}_nT_0\sqrt{\frac{\mu}{1+p\left(\mu-1\right)}} \tag{7}$$

where $p = \frac{{}_nK_h}{{}_nK_0}$ denotes the hardening stiffness ratio; $\mu = \frac{{}_nD_t}{{}_nD_y}$ denotes the ductility ratio when the target deformation is assumed as ${}_nD_t$; ${}_nD_y$ is the yielding deformation; and ${}_nD_0$ and ${}_nA_0$ denote the primarily estimated deformation and force corresponding to the initial period ${}_nT_0$ and initial damping ratio ${}_nh_0$ (=0.02), respectively. They are updated by Eqs. (8) and (9) till a convergence is reached, where ${}_nR_d$ and ${}_nR_a$ are the deformation and force reduction factors:

$$ {}_nD = {}_nR_d\,{}_nD_0,\ {}_nR_d = \begin{cases} \dfrac{{}_nT_{eq}}{{}_nT_0}\,{}_nD_h & T_l \le {}_nT_0 \le {}_nT_{eq} \\ \dfrac{{}_nT_{eq}}{{}_nT_0}\,{}_nD_h\,\dfrac{T_l\left(2\,{}_nT_{eq} - {}_nT_l\right) - \left({}_nT_0\right)^2}{2\left({}_nT_{eq} - {}_nT_0\right){}_nT_0} & {}_nT_0 \le T_l \le {}_nT_{eq},\ T_l = 0.864\ \text{s} \\ \dfrac{{}_nT_{eq}}{{}_nT_0}\,{}_nD_h\,\dfrac{{}_nT_{eq} + {}_nT_0}{2\,{}_nT_0} & {}_nT_0 \le {}_nT_{eq} \le T_l \end{cases} \tag{8} $$

${}_nD_h = \sqrt{\dfrac{1+\alpha\,{}_nh_0}{1+\alpha\,{}_nh_{eq}}}$, α is an empirical value, set as 25.

$$ {}_nA = {}_nR_a\,{}_nA_0,\ {}_nR_a = {}_nR_d\left(\frac{{}_nT_f}{{}_nT_{eq}}\right)^2 \tag{9} $$

Step 6. Inversely convert ${}_nD$ to the peak *i*th floor displacement ${}_nu_i$ in the inelastic MDOF system.

Step 7. From the pushover database (step 2), extract values of desired response ${}_nr$ at *i*th floor displacement equal to ${}_nu_i$.

Step 8. Repeat steps 3 to 7 for as many modes as required for sufficient accuracy.

Step 9. Determine the total seismic response by combining the peak modal responses using a modal combination rule.

The MPA procedure can also be used to estimate internal forces in those structural members that remain within their linearly elastic range, but not in those that deform into the inelastic range. In the latter case, the member forces are estimated from the total member deformations.

REFERENCE FLOOR

The assumption of invariable mode shapes before and after the yielding mechanism occurs might not be satisfied, particularly for the spine frame structures, because the yielding deformation concentrates in dampers that are equipped at specific stories. Therefore, the relationship between the different floor displacement and base shear obtained from the pushover analysis of the original structure results in a different hardening stiffness ratio (even reversal deformation) in the force-deformation curve of the corresponding SDOF system, as shown in Fig. 5 (a).

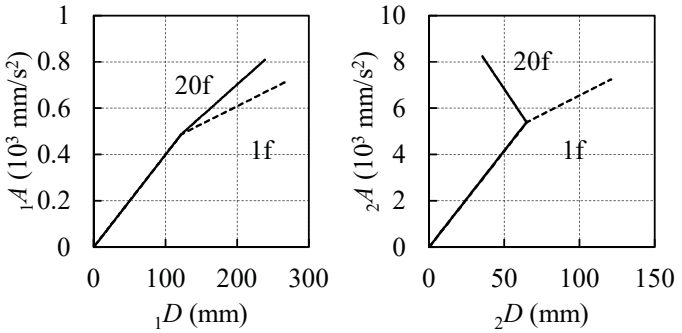

(1) First mode (2) Second mode

Figure 5. SDOF force-deformation (A-D) curves obtained by using 1st or 20th floor as ref. floor (model: 20-story Cnt-Ksf0.3-Kdf1.0, input: BCJ-L2)

Previous researchers also observed the "reversal" curves in the higher-mode pushover analysis and suggested to use lower floors as the reference floor. (R. K. Chopra et al. 2005) For the spine frame structures, the estimation of responses using the SDOF is more conservative when the hardening stiffness ratio is larger. For the first mode, the top floor gives the largest hardening stiffness ratio; for the second mode, the first floor gives almost the largest hardening stiffness ratio (Fig. 6). Similar results are obtained for the Sgt2 models. These two floors are determined as the reference floors for first mode and second mode, respectively.

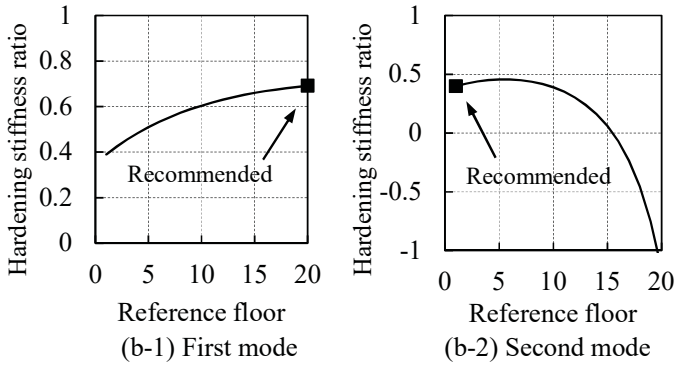

(b-1) First mode (b-2) Second mode

Figure 6. Hardening stiffness ratio obtained by using different ref. floors (model: 20-story Cnt-Ksf0.3-Kdf1.0, input: BCJ-L2)

SEISMIC EVALUATION BASED ON RESPONSE SPECTRUM ANALYSIS

EVALUATION PROCEDURE

In the previous paper (X. Chen et al. 2017), the authors proposed a simplified evaluation method based on equivalent linearization techniques and response spectrum analysis (RSA) for low-rise spine frame structures. It was verified that this method provides enough accuracy when the key structural parameters are in a regular range, which has been quantified in the

previous paper. In this paper, the modified procedure by including the higher-modes contribution to the seismic performance of high-rise buildings (Fig. 7) is proposed as follows:

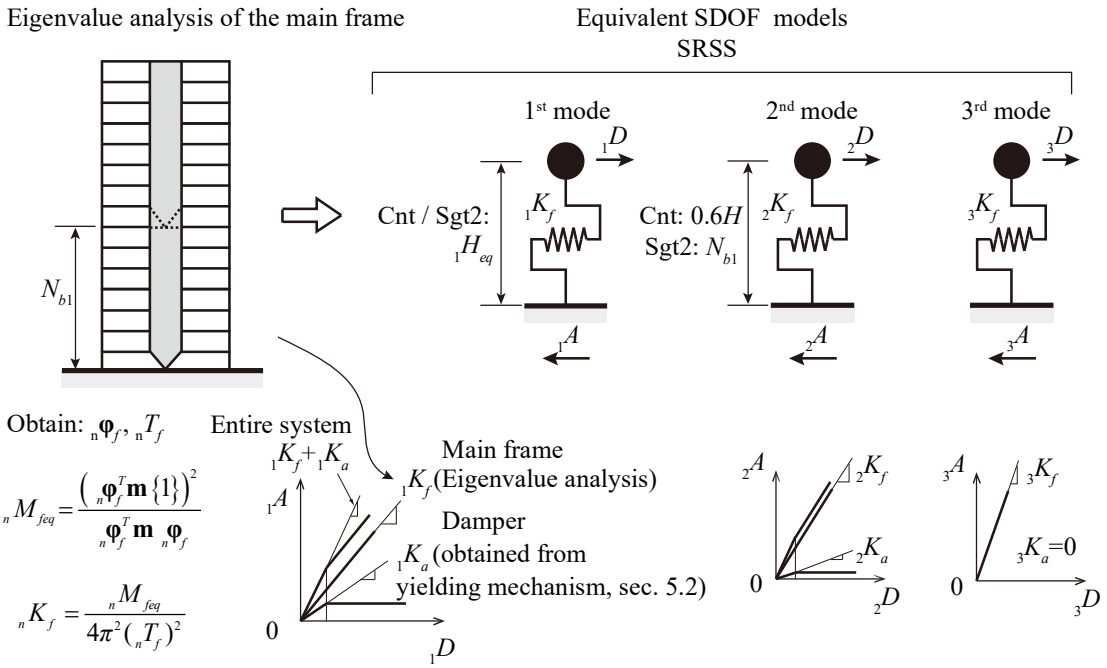

Figure 7. Multi-mode response spectrum analysis for the spine frame structures

Step 1. Compute the natural periods, ${}_nT_f$, and modes, ${}_n\boldsymbol{\varphi}_f$, for the linearly elastic vibration of the main frame without BRCs. Obtain the elastic force-deformation ${}_nA-{}_nD$ relation with stiffness ${}_nK_f$ for the SDOF system by utilizing Eq. (5).

Step 2. Evaluate the elastic modal responses ${}_nr_f$ of the main frame with an inherent damping ratio of 0.02. To evaluate the forces of the structural members, an elastic pushover analysis using the lateral force distribution ${}_n\mathbf{q}_f{}^*$ is required. (${}_n\mathbf{q}_f{}^* = \mathbf{m}\ {}_n\boldsymbol{\varphi}_f$)

Step 3. For the *n*-th mode, compute the additional stiffness ${}_nK_a$ and yielding deformation ${}_nD_y$ contributed by the BRCs. Determine the system initial stiffness ${}_nK_{f+a} = {}_nK_f + {}_nK_a$. The system hardening stiffness equals to ${}_nK_f$ obtained from step 1.

Step 4. Compute the deformation and force reduction factors, ${}_nR_d$ and ${}_nR_a$, by utilizing Eqs. (6)–(9) iteratively, where ${}_nK_0$ and ${}_nK_h$ are replaced with ${}_nK_{f+a}$ and ${}_nK_f$. Eq. (8) is replaced with Eq. (8*), because the main frame herein excludes the dampers (${}_nT_{f+a}$ in RSA equals to ${}_nT_0$ in MPA; both are the initial stiffness of the whole system)

269
$$ {}_nR_d = \begin{cases} \dfrac{{}_nT_{eq}}{{}_nT_f}\,{}_nD_h & T_l \le {}_nT_{f+a} \le {}_nT_{eq} \le {}_nT_f \\ \dfrac{{}_nT_{eq}}{{}_nT_f}\,{}_nD_h \dfrac{T_l\left(2\,{}_nT_{eq}-T_l\right)-{}_nT_{f+a}{}^2}{2\left({}_nT_{eq}-{}_nT_{f+a}\right)T_l} & {}_nT_{f+a} \le T_l \le {}_nT_{eq} \le {}_nT_f \\ \dfrac{{}_nT_{eq}}{{}_nT_f}\,{}_nD_h \dfrac{{}_nT_{eq}+{}_nT_{f+a}}{2T_l} & {}_nT_{f+a} \le {}_nT_{eq} \le T_l \le {}_nT_f \\ \dfrac{{}_nT_{eq}}{{}_nT_f}\,{}_nD_h \dfrac{{}_nT_{eq}+{}_nT_{f+a}}{2\,{}_nT_f} & {}_nT_{f+a} \le {}_nT_{eq} \le {}_nT_f \le T_l \end{cases} \quad (8*) $$

270 Step 5. Evaluate the desired responses of the original structure by multiplying ${}_nR_d$, or ${}_nR_a$.

271 Step 6. Repeat steps 3 to 5 for as many modes as required for sufficient accuracy.

272 Step 7. Determine the total seismic response by combining the peak modal responses using
273 the SRSS modal combination rule.

274 Note that in the RSA procedure, the static pushover analysis is not necessary for evaluating
275 the maximum deformation and story shear of the entire structure, unless the results of structural
276 member-level forces are desired. The effect of damper stiffness could be simply estimated by
277 formula calculation without numerical analysis, which is more convenient compared to the
278 MPA procedure.

279 **ESTIMATION OF DAMPER STIFFNESS**

280 Generally, the connection elements have a significant influence on the effectiveness of
281 damping devices, reducing the imposed local deformations and achieved damping for a given
282 level of drift. For controlled spine frame structures, the spine frame flexural stiffness reduces
283 the effective damper stiffness and it must be accounted for. To isolate the spine frame stiffness
284 in the member-by-member model, an eigenvalue analysis is first conducted with the dampers
285 substituted with rigid elements (Fig. 8 (a)), and then with the dampers removed (Fig. 8 (b)).
286 Thus, the stiffness of the spine frame K_c can be isolated from the frame K_f by subtracting the
287 results of the first pushover analysis ($K_c + K_f$) from the second K_f. The local damper stiffness
288 K_d is determined in the following sections. Finally, the stiffness of the entire structure is
289 expressed by Eq. (10)

290
$$ K_a = \frac{1}{\dfrac{1}{K_d} + \dfrac{1}{K_R - K_f}} \quad (10) $$

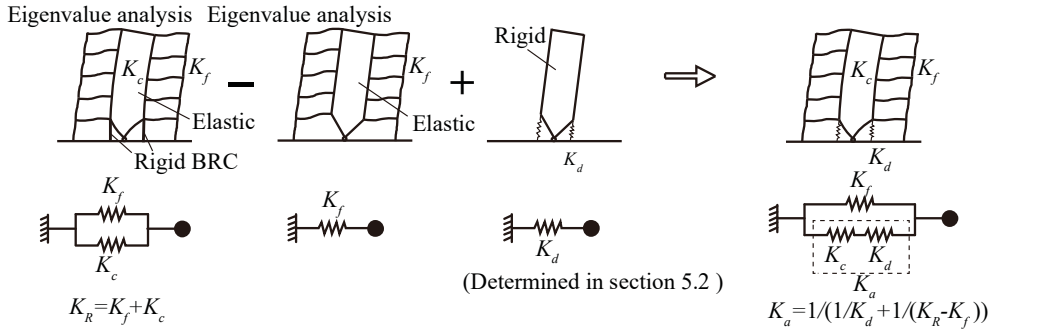

(a) Condition R (b) Condition N (c) Stiffness of dampers (d) Additional stiffness due to dampers

Figure 8. Computation of additional stiffness considering flexural deformation of spine frames

Damper stiffness and yielding deformation of Cnt models

The estimation of damper stiffness is essential for ensuring the accuracy of the RSA results because the stiffness of the main frame K_f is obtained directly from the eigenvalue analysis, which is regarded as accurate. The damper stiffness and yielding deformation in the first- or second-mode SDOF system of the Cnt models is calculated by Eq. (11) (a) and (b). The damper stiffness in modes higher than the second mode can be ignored as the generated error in total response is usually less than 0.1% for spine frame structures.

$$ {}_iK_d = \frac{F_{BRC\_y}\left(b\right)^2}{2u_{BRC\_y}\left({}_iH_d\right)^2},\ i=1,2\ \text{(a)};\ {}_iD_{dy} = \frac{2u_{BRC\_y}}{b\,{}_i\beta\,{}_i\varphi_1/h_1}\cdot\frac{{}_iK_a}{{}_iK_d},\ i=1,2\ \text{(b)} \tag{11} $$

where, ${}_iH_d$ is the height of the equivalent damping force location: ${}_1H_d = {}_1H_{eq}$ for the first mode; ${}_2H_d = 0.6H$ for the second mode. ${}_iK_d$ is the damper stiffness in the first-mode (i=1) or second-mode (i=2) of the SDOF system; F_{BRC_y} and u_{BRC_y} are the yielding axial force and yielding deformation of a single BRC, respectively; b is the lateral distance between a pair of BRCs; and h_1 is the height of the first story.

The equivalent force represents a concentrated horizontal force possessing the same value with shear force allocated by the additional damper system and could generate an identical overturning moment as the distributed horizontal forces. The elastic modal stiffness obtained by MPA is utilized to calculate ${}_iH_d$ for the first- and second-mode SDOF systems in RSA in order to validate Eq. (11). Fig. 9 shows that ${}_1H_d$ is almost identical with ${}_1H_{eq}$ and the effects of K_s/K_f and K_d/K_f on both are negligible. Initial stiffness, yielding deformation and maximum deformation evaluated by using RSA and MPA are almost identical. (Appendix A, Fig A.1)

$_2H_d / H$ slightly increases with K_s/K_f and reaches 0.6 when K_s/K_f=2.0. Although assuming that $_2H_d = 0.6H$ causes a larger error when K_s/K_f is smaller, such difference has little effect on the initial stiffness or yielding deformation of the second mode vibration of the system (Appendix A, Fig A.2), because main frame stiffness rather than the damper stiffness is dominant in the second-mode stiffness. (ex. the RSA curve in Fig 10 (b))

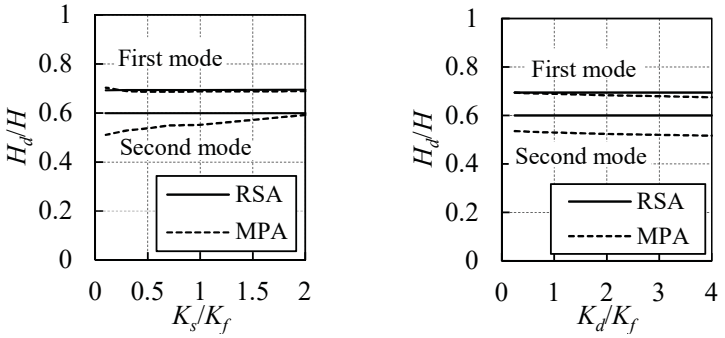

(a) H_d/H with various K_s/K_f (K_d/K_f=1.0) (b) H_d/H with various K_d/K_f (K_s/K_f=0.3)

Figure 9. Verification of H_d for Cnt models by MPA method

Since the main frame stiffness is accurate in the RSA method, we can use it to validate the main frame stiffness obtained by the MPA method. Fig. 10(b) compares the detailed A-D curves of a Cnt model obtained by RSA and MPA methods. We can see that hardening stiffness, i.e., the stiffness of the main frame, obtained by the eigenvalue analysis in RSA is much larger than the MPA result, which is mainly because the lateral force distribution utilized in the MPA is kept proportional to the elastic force distribution, and it underestimates the post-yield stiffness. Comparison on the hardening stiffness of other Cnt models can be found in Appendix A, Figs A.1 and A.2.

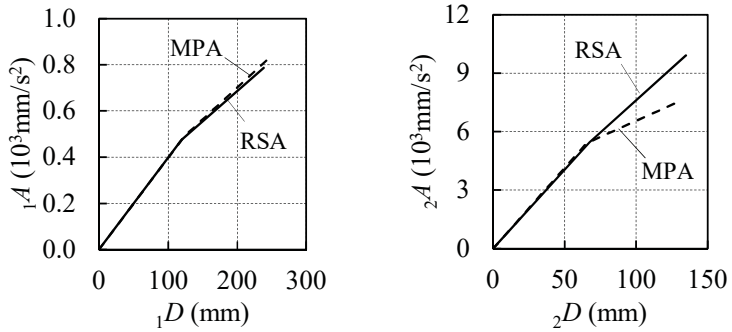

(a) First mode (b) Second mode

Figure 10. Comparison between RSA and MPA in SDOF A-D curves of Cnt models (model: 20-story Cnt-Ksf0.3-Kdf1.0)

Damper stiffness and yielding deformation of Sgt models

The calculation of the damper stiffness ${}_iK_d$ for the Sgt2 models is relatively more complicated than for the Cnt models. As for the first mode, the elastic deformations of both BRC1s and BRC2s are taken into account in the calculation of the dampers stiffness (Eqs. (12)–(14)). ${}_1H_{eq}$ is assumed as the location of the equivalent concentration force. As for the second mode, the BRC2s are assumed to yield initially because the MPA results show that they make little contribution to the overall damper stiffness (Eq. (15)). Detailed explanation on the yielding mechanism of dampers in the Sgt2 models is in Appendix B. The height of the BRC2s H_{Nb} is assumed as the location of the equivalent concentration force, as shown in Fig. 11. Yielding deformation are calculated by Eq. (11) (b). Fig. 12 shows that ${}_1H_{eq}$ and H_{Nb} match well with the height obtained from the MPA method.

$$\begin{cases} {}_1\theta_2 = {}_1M_2 / K_{d2} \\ {}_1M_2 = {}_1Q_{dy}\left({}_1H_{eq} - H_{Nb}\right) \\ {}_1\delta_2 = {}_1\theta_2\left({}_1H_{eq} - H_{Nb}\right) \end{cases} \longrightarrow {}_1\delta_2 = \frac{{}_1Q_{dy}\left({}_1H_{eq} - H_{Nb}\right)^2}{K_{d2}} \tag{12}$$

$$\begin{cases} {}_1\theta_1 = M_{dy1} / K_{d1} \\ M_{dy1} = {}_1Q_{dy}\,{}_1H_{eq} \\ {}_1\delta_1 = {}_1\theta_1 \cdot {}_1H_{eq} \end{cases} \longrightarrow {}_1\delta_1 = \frac{{}_1Q_{dy}\,{}_1H_{eq}^{\,2}}{K_{d1}} \tag{13}$$

$${}_1K_d = \frac{{}_1Q_{dy}}{\left({}_1\delta_1 + {}_1\delta_2\right){}_1M_{eq}} = \frac{1}{\dfrac{{}_1H_{eq}^{\,2}}{K_{d1}} + \dfrac{\left({}_1H_{eq} - H_{Nb}\right)^2}{K_{d2}}} \cdot \frac{1}{{}_1M_{eq}} \tag{14}$$

$${}_2K_d = \frac{M_{dy1}}{\theta_{dy1}\left(H_{Nb}\right)^2\,{}_2M_{eq}} = \frac{K_{d1}}{\left(H_{Nb}\right)^2\,{}_2M_{eq}} \tag{15}$$

where K_{d1} and K_{d2} are the rotational stiffnesses of the elasto-plastic hinges formed by BRC1s and BRC2s; M_{dy1} is the yielding moment of hinge BRC1; ${}_1Q_{dy}$ is the lateral force at a height of ${}_1H_{eq}$, when hinge BRC1 yields in 1st-mode SDOF system; and ${}_1M_2$ is the elastic moment of hinge BRC2, when subjected to the lateral force ${}_1Q_{dy}$ in the 1st-mode SDOF system.

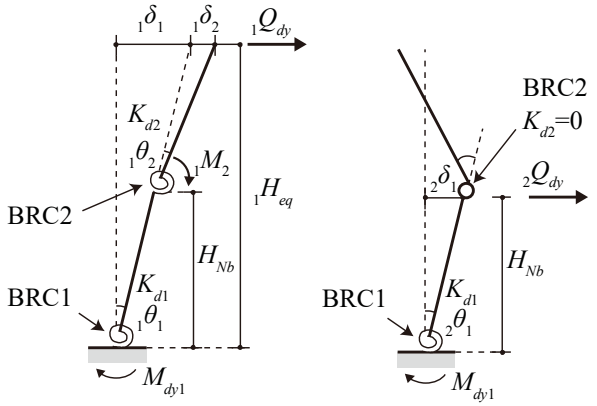

(a) First mode (b) Second mode

Figure 11. Concept of computing damper stiffness of a Sgt2 model

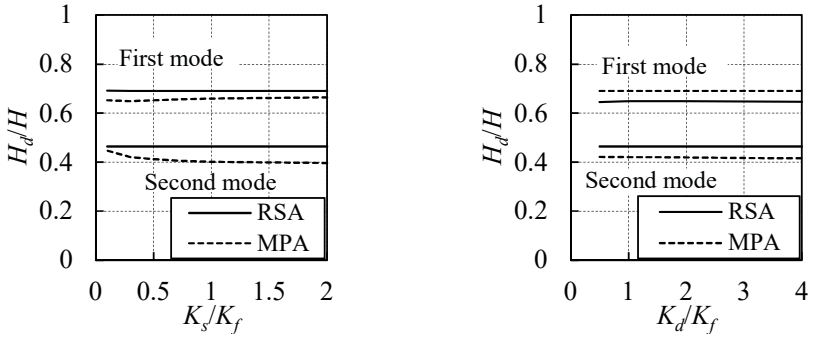

(a) H_d/H with various K_s/K_f (K_d/K_f=1.0) (b) H_d/H with various K_d/K_f (K_s/K_f=0.3)

Figure 12. Verification of H_d for Sgt2 models by MPA method

Generally, the initial stiffness and yielding deformation of the 1st- and 2nd-mode SDOF systems determined by the RSA are in good agreement with those determined by the MPA when K_s/K_f =0.0–2.0 and K_{d1}/K_f =0.0–2.0. (Appendix A, Figs A.3 and A.4, (a-1), (a-2), (b-1), (b-2)) The second-mode hardening stiffness of the RSA is much larger than that of the MPA. Similar to the Cnt models, the main reason is that the lateral force distribution utilized in the MPA is kept proportional to the elastic force distribution and it underestimates the post-yield stiffness. As a result, the difference between the RSA and MPA in hardening stiffness increases as K_{d1}/K_f increases. (Appendix A, Figs A.3 and A.4, (a-3), (b-3))

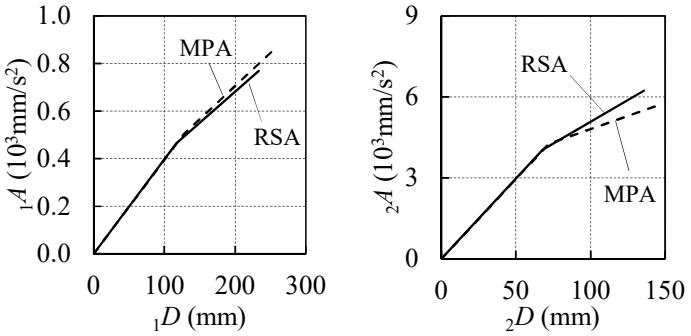

(a) First mode (b) Second mode

Figure 13. Comparison between RSA and MPA in SDOF A-D curves of Sgt2 models (model: 20-story Sgt2-Ksf0.3-Kdf1.0-0.5 model)

PARAMETRIC STUDY OF EACH CONTROLLED SPINE SYSTEM USING TIME-HISTORY ANALYSIS

SEISMIC BEHAVIOR OF CNT MODELS

In this chapter, response characteristics of each spine system proposed in Fig.2 are compared and discussed using the parameters K_d, K_f, and K_s as defined in previous chapters. The averaged results of story drift ratio (SDR), story shear ratio (story shear normalized by the seismic weight of the structure) obtained by time-history analysis with various inputs are summarized in Fig. 14 along with the first mode natural period of the SW and Cnt models. The higher mode effect is observed in the shear force distribution of the 20- to 30-story buildings. Except for the SDR of the 5-story building, both the SDR and shear force response in the controlled Cnt models are smaller than in the SW models. The main reason for this is the shift period of the softer Cnt models, particularly for the taller buildings. The SDR of the Cnt models is more uniformly distributed than in the SW models.

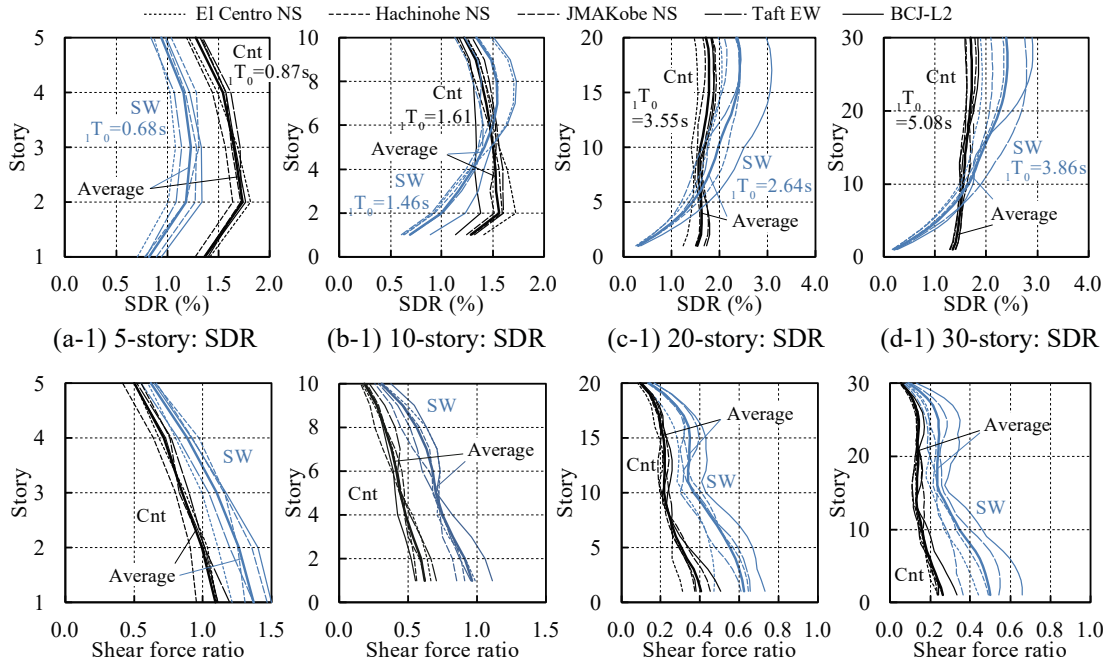

Figure 14. Seismic performance of Cnt and SW models with various heights

The effects of spine-to-moment frame stiffness ratio, K_s/K_f, and damper-to-moment frame stiffness ratio, K_d/K_f, on the seismic response of the 5-, 10-, 20-, and 30-story Cnt models were studied based on the time-history analysis. Fig. 15 shows the average results obtained from five ground motions input. As shown in Fig. 15(a), the maximum SDR decreases as K_s/K_f increases, and tends to be constant after K_s/K_f exceeds 1.0. The base shear of the 5-story model is relatively independent of K_s/K_f, and the base shear of the 10-story model increases till K_s/K_f reaches 1.0, while the base shear of the 20- and 30-story buildings increases slowly when K_s/K_f is increasing. The stiff spine frame has an effect in achieving a more uniform deformation distribution, even for structures as tall as 30 stories. Fig. 15(b) shows that, generally, both the SDR and base shear of the four models decrease when K_d/K_f increases from 0 to 2.0, and then they tend to be constant despite of the damper stiffness. This indicates that increasing the damper stiffness is not always effective to reduce the seismic performance of the buildings.

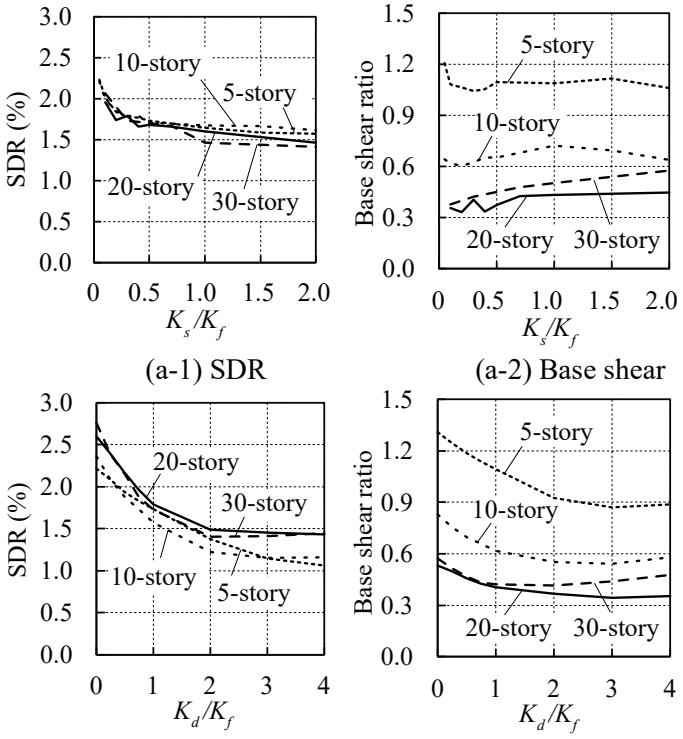

Figure 15. Seismic performance of Cnt and SW models with various heights: (a) Effect of K_s/K_f (K_d/K_f=1.0) (b) Effect of K_d/K_f (K_s/K_f=1.0)

SEISMIC BEHAVIOR AND OPTIMAL STRUCTURAL PROPERTIES OF SGT2 MODELS

Time-history analysis with five ground motions was carried out to investigate the seismic behavior and optimal structural properties of the Sgt models. Fig. 16 illustrates the maximum SDR and base shear of a typical 20-story Sgt2 model, obtained by a time-history analysis with the BCJ-L2 input. The story number of the bottom spine, N_{b1}, ranges from 2 to 19; and K_s/K_f varies among 0.1, 0.3, 0.5, 0.7, and 1.0. Both K_{d1}/K_f and K_{d2}/K_f are kept constant at 1.0. When K_s/K_f is 0.1, the curves of SDR and base shear are almost flat, indicating that the spine frame is too soft to reduce the response of the moment frame. When K_s/K_f is not less than 0.3, the maximum SDRs of the Sgt2 models achieve the smallest values when N_{b1} is around 10–15, but are still similar to those of the Cnt models, as shown in Fig. 16(a). From Fig. 16(b) we could see that the base shear of the whole structure reaches the smallest value when N_{b1} is around 10–15. As for the Sgt2 models with various K_s/K_f and K_d/K_f, the optimal configurations could be with N_{b1} ranging from 10 to 15.

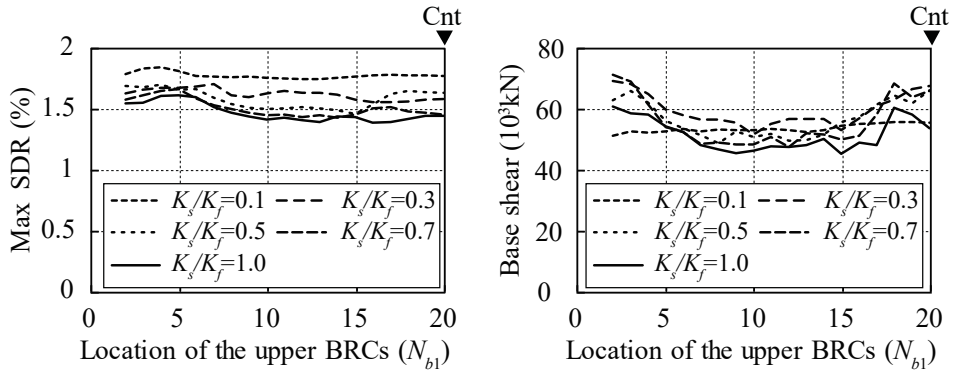

(a) Effect of N_{b1} on SDR (b) Effect of N_{b1} on base shear

Figure 16. Effect of K_s/K_f and N_{b1} on seismic performance of Sgt2 models (model: 20-story Sgt2-Ksf0.3-Kdf1.0-1.0, input ground motion: BCJ-L2)

As two examples among the optimal cases, the models Sgt2-Ksf0.3-Nb10 and Sgt2-Ksf0.3-Nb15 were used to search the optimal damper stiffness of the upper spine frame. Figs. 17(b) and (d) show the average results of maximum SDR and base shear of the Sgt2 and Cnt models, obtained from the time-history analysis.

Generally, in the 0.5–1.0 range of K_{d1}/K_f, the SDR of the Sgt2 model is less than that of the Cnt model, and the base shear is reduced by almost 25% in the Sgt2 model. The effect when K_{d2}/K_{d1} (defined as R_{Kd}) is varied among 0.5, 0.75, and 1.0 was also studied. However, the effect of R_{Kd} on the SDR is negligible in both models. Similar results have been observed for the base shear when K_{d1}/K_f is less than 1.0. When K_{d1}/K_f is larger than 1.0, a R_{Kd} of 0.5 gives the smallest base shear. Figs. 17(a) and (c) show the SDR and story shear distribution of two Sgt2 models, Sgt2-Ksf0.3-Nb10-Kdf1.0-0.5 and Sgt2-Ksf0.3-Nb15-Kdf1.0-0.5, along with the Cnt-Ksf0.3-Kdf1.0 model. We could observe a more uniformly distributed SDR and linearly distributed story shear in the Sgt2 models. Moreover, both the maximum SDR and base shear of the Sgt2 models are reduced compared to those of the Cnt model. The Sgt2 and Cnt models possessing the same total size of dampers were also examined. The Sgt2-Ksf0.3-Nb10-Kdf0.5-0.5, Sgt2-Ksf0.3-Nb15-Kdf0.5-0.5, and Cnt-Ksf0.3-Kdf1.0 models were compared, and the results showed that the base shear force could be reduced by adopting the Sgt2 models.

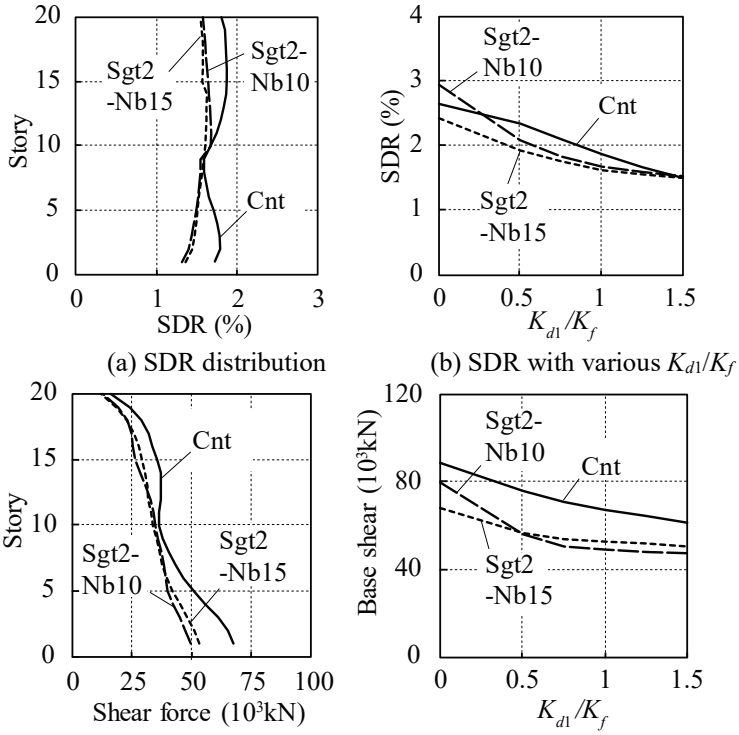

(a) SDR distribution (b) SDR with various K_{d1}/K_f

(c) Shear force distribution (d) Base shear with various K_{d1}/K_f

Figure 17. Comparison between 20-story Cnt and Sgt2 models (K_s/K_f =0.3 and K_{d2}/K_{d1}=0.5 in a–d, K_{d1}/K_f =1.0 in a & c, average results)

The effects of K_{d1}/K_f and R_{kd} in the 30-story models were also investigated, as shown in Figs. 18(a)–(d). The effects of N_{b1} in the 30-story models are almost the same as those in the 20-story models. The optimal value of N_{b1} is around 15–23, 50%–75% of the total height, in which both the SDR and base shear achieve the smallest response.

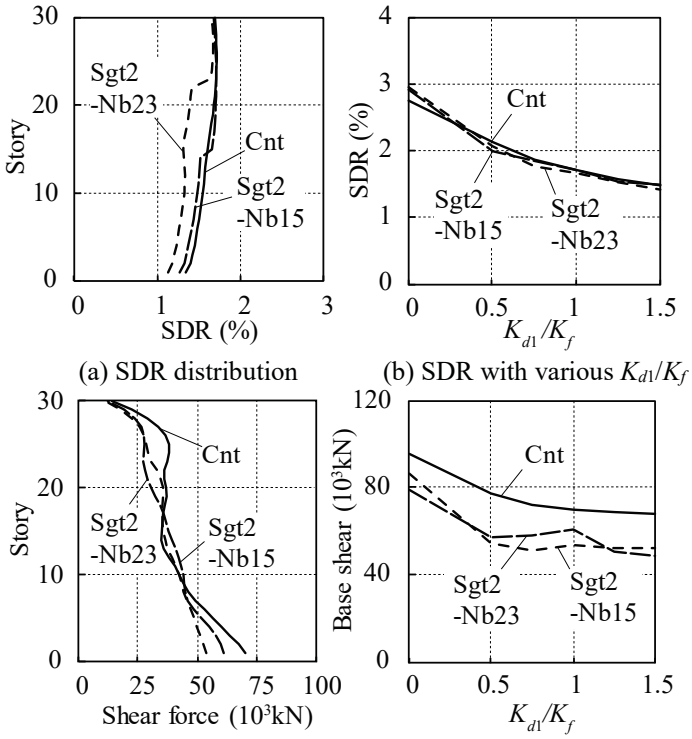

(a) SDR distribution (b) SDR with various K_{d1}/K_f

(c) Shear force distribution (d) Base shear with various K_{d1}/K_f

Figure 18. Comparison between 30-story Cnt and Sgt2 models (K_s/K_f =0.3 and K_{d2}/K_{d1}=0.5 in a–d, K_{d1}/K_f =1.0 in a & c, average results)

SEISMIC BEHAVIOR AND OPTIMAL STRUCTURAL PROPERTIES OF SGT3 MODELS

Three-segment-spine (Sgt3) models were also tried for the 30-story building. Time-history analyses of the Sgt3 models with different segmentations were carried out. In those models, N_{b1} ranges from 10 to 20, and N_{b2} ranges from (N_{b1}+4) to 28, and K_s/K_f=0.3, K_{d1}/K_f= K_{d2}/K_f= K_{d3}/K_f =1.0. The results of the analyses show that the different configurations of those Sgt3 models do not substantially change the SDR response, as shown in Fig. 19.

To compare the Sgt3 models with the Sgt2 models, for each N_{b1} of the Sgt3 models, we selected the cases in which the SDR was the smallest among different N_{b2}, and the results are shown in Figs. 20(a) and (b). The difference in both the SDR and base shear results between the Sgt2 and Sgt3 models of the 30-story building is negligible. This is because the BRCs of the top spine (BRC3) do not significantly work, which is indicated by the small ductility ratio shown in Fig. 20(c). Therefore, the three-segment-spine-frame structure is not effective and not recommended for high-rise buildings of less than 30 stories.

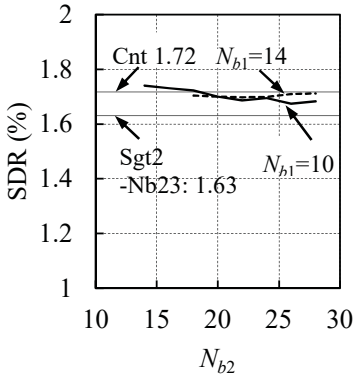

Figure 19. SDR of Sgt3 models with various N_{b1} and N_{b2} (input ground motion: BCJ-L2)

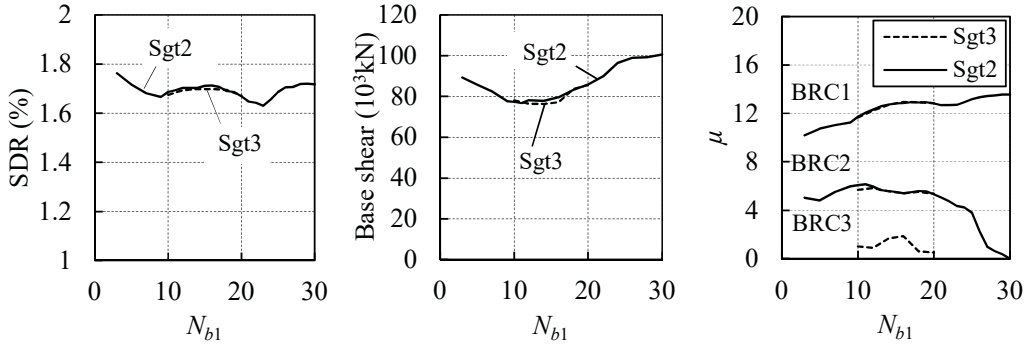

(a) SDR (b) Base shear (c) Ductility ratio

Figure 20. Comparison between the Sgt2 model and the optimal Sgt3 models (input ground motion: BCJ-L2)

VERIFICATION OF THE PROPOSED EVALUATION METHODS

In the following, validities of the proposed response evaluation methods are discussed. Displacement and force distribution of each component of the Cnt and Sgt2 models which were evaluated by MPA method was compared with the results obtained from time-history analysis (THA). As shown in Fig. 21, the responses estimated by using the MPA procedure considering three modes agreed well with the results of the time-history analysis. From the estimated modal response, we could understand that the first three modes provide enough accuracy for evaluating the seismic performance of both the Cnt and Sgt2 models. Besides, the first mode response is dominated in the floor displacement, story drift ratio, and shear force and overturning moment of the moment frames. The second mode contributed to a significant response in story shear and bending moment of the spine frames (Fig. 21 (g)). The responses subjected to other input waves gave similar results.

The MPA results including the first three modes of the Sgt2 and Cnt models show that the force of the spine frames is significantly reduced in the Sgt2 models, whereas the force of the moment frames remains at a similar level, compared to those of the Cnt models (Figs. 21 (e) and (f) vs. (b) and (c)). Meanwhile, increased moment demand for the moment frames and shear force demand for both moment and spine frames, at approximately the BRC2s level, are required (Figs. 21(b), (c), and (e)).

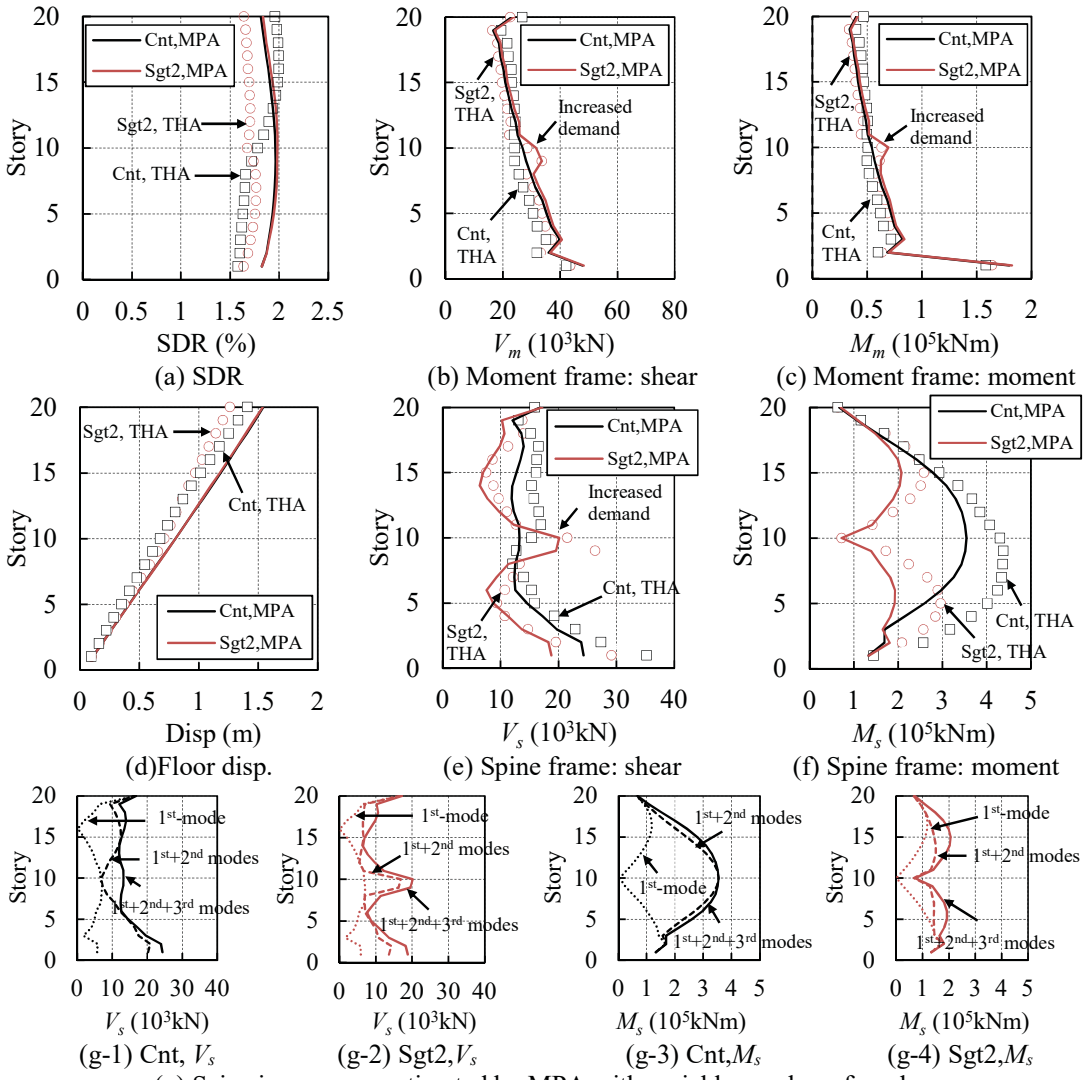

Figure 21. Seismic response of a Cnt and a Sgt2 model estimated by MPA and THA (models: 20-story Cnt-Ksf0.3-Kdf1.0 and 20-story Sgt2-Ksf0.3-Kdf1.0-0.5, input: BCJ-L2)

Displacement and force distribution of each component of the Cnt and Sgt2 models which were evaluated by RSA method was compared with the results obtained from time-history

analysis. As shown in Fig. 22, the RSA method considering three modes gives a good estimation for the deformation responses of both the Cnt and Sgt2 models. The 'two-stage' shaped SDR distribution is well captured in the Sgt2 model (Fig 22(a)), because the deformation shape is assumed to be proportional to the mode shape of the main frame, excluding the dampers. Contrary to the MPA method, the RSA method gives a slightly conservative estimation of the forces in the spine frames.

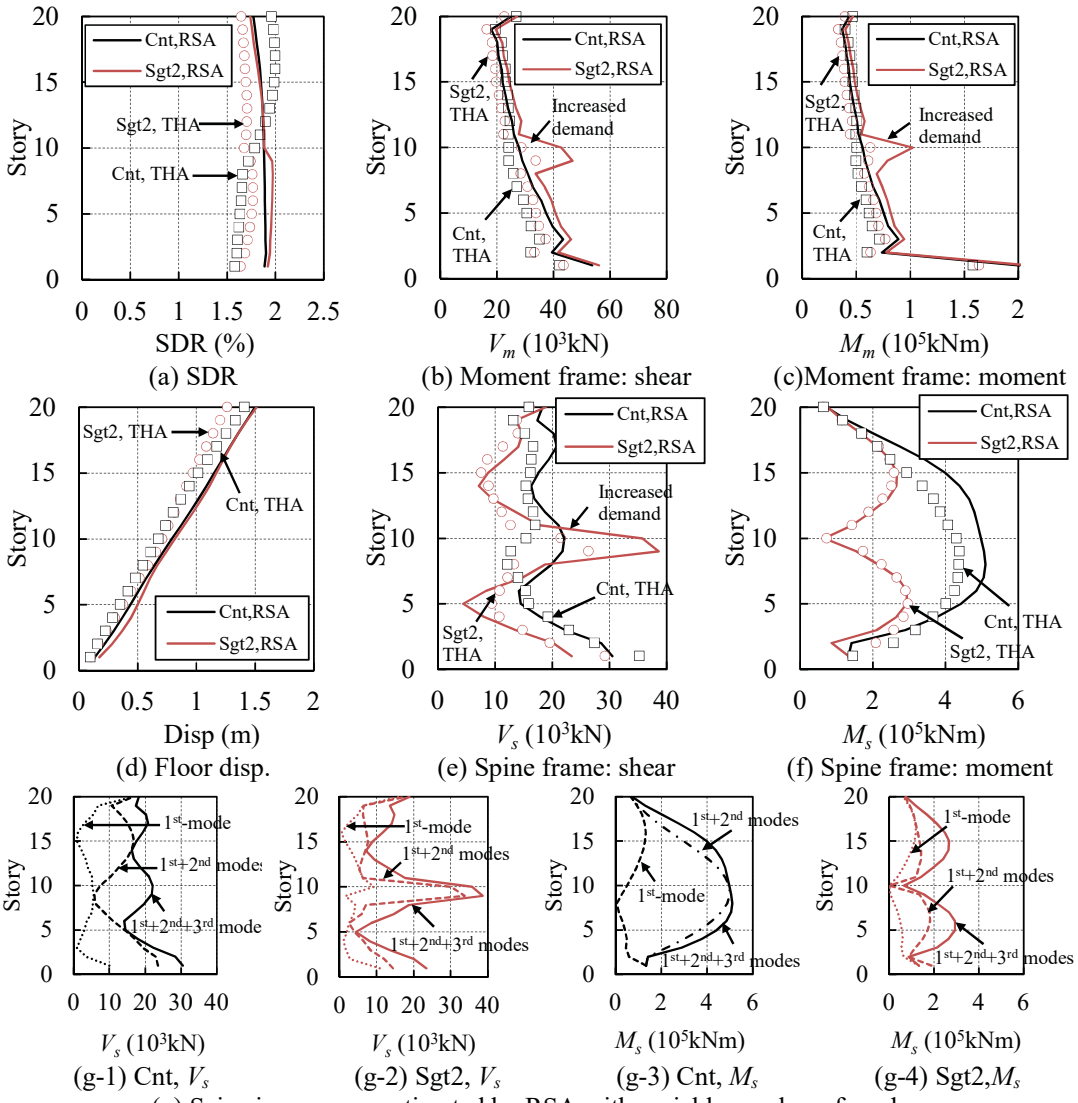

Figure 22. Seismic response of a Cnt and a Sgt2 model estimated by RSA and THA (models: 20-story Cnt-Ksf0.3-Kdf1.0 and 20-story Sgt2-Ksf0.3-Kdf1.0-0.5, input: BCJ-L2)

Fig. 23 compares the seismic response of Cnt models evaluated by using the RSA and MPA methods to the THA along the K_s/K_f and K_d/K_f indexes. Both the RSA and MPA methods provide a good estimation with appropriate conservatism on the maximum SDR, roof displacement, shear force, and overturning moment of the moment frames of the Cnt models when K_s/K_f =0.1–2.0 and K_d/K_f =0–1.0. However, the error of the forces in the moment frame increased when K_d/K_f increases, particularly when $K_d/K_f \geq 2.0$, as shown in Figs. 23(b-3) and (b-5). The main source of error in the MPA procedure is the reference floor. Choosing a more representative reference floor, rather than the most conservative one, could greatly improve the accuracy. The main source of error in the RSA procedure could be the post-yield response distribution. When the input earthquake intensity increased (and the plasticity of the structure further developed), the difference between the RSA and THA decreased. Therefore, the RSA procedure provides a better estimation for structures developing into sufficient plasticity, or structures in which the response distribution did not change much after the formation of the yielding mechanism. These results also indicate that the dampers could decrease the peak force response not only by introducing additional damping, but also by changing the distribution pattern of the spine frame structures.

To modify this error, a modification factor γ (Eq. (16)) is introduced for the estimation of forces of the moment frames in the RSA procedure. Figs. 23 (b-3) and (b-5) show the modified estimation results.

$$\gamma = 1 - 0.15K_d / K_f \tag{16}$$

As for the Sgt2 models, the RSA procedure provided a relatively more conservative estimation for both deformation and force, compared to the MPA procedure (Fig. 24). Despite the values of K_s/K_f and K_{d1}/K_f, the RSA and MPA estimated the maximum SDR and roof displacement well, with proper conservatism. As for the force responses, the RSA provided a better estimation for the spine frames compared to the MPA, particularly when $K_{d1}/K_f \leqslant 2.0$. Nevertheless, similarly with the Cnt models, the modification factor defined for forces of moment frame of the Cnt models is also utilized for those of the Sgt models, and it gives a good accuracy.

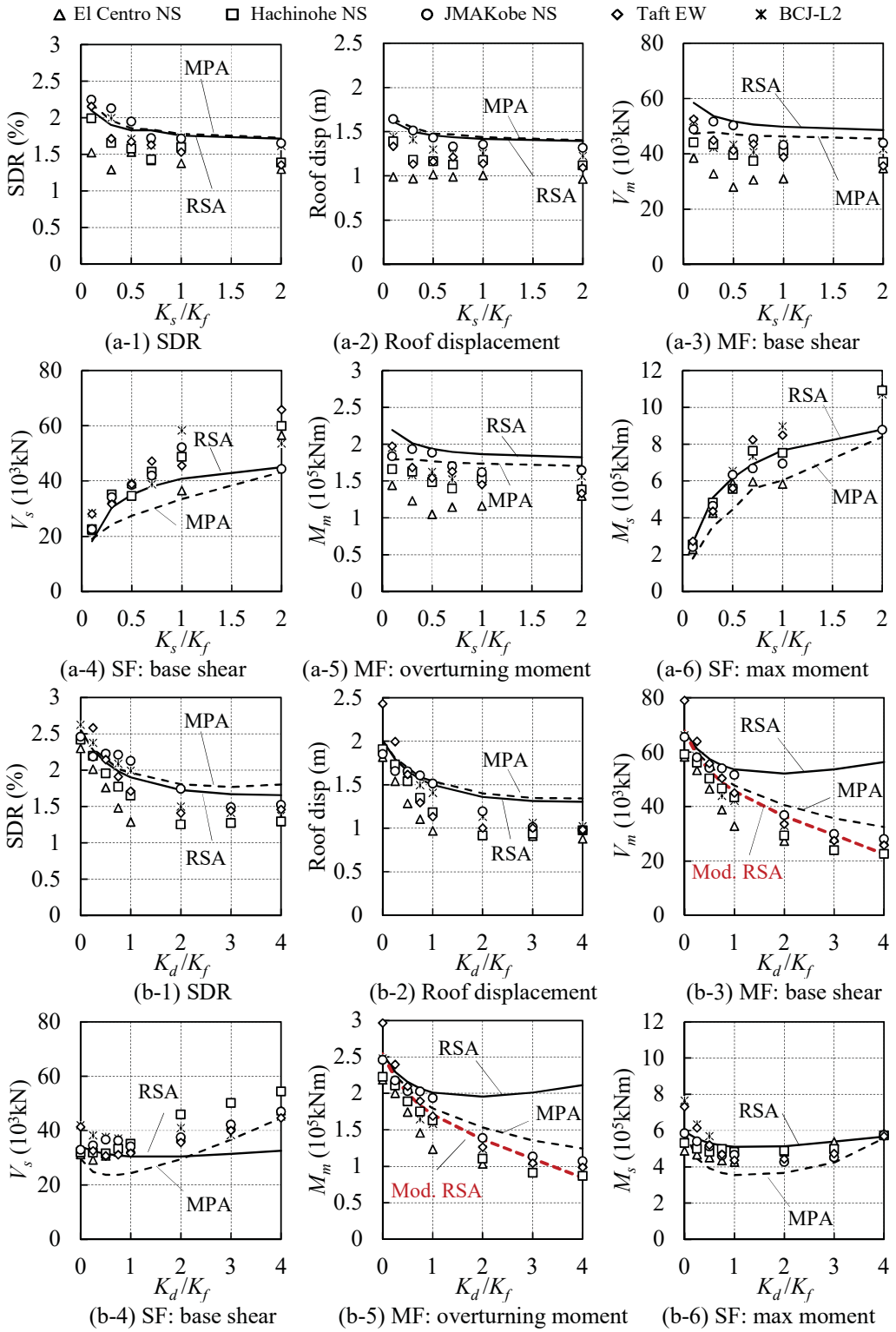

Figure 23. Comparison of RSA, MPA, and THA on seismic response of Cnt models: (a) with various K_s/K_f(K_d/K_f=1.0); (b) with various K_d/K_f(K_s/K_f=0.3)

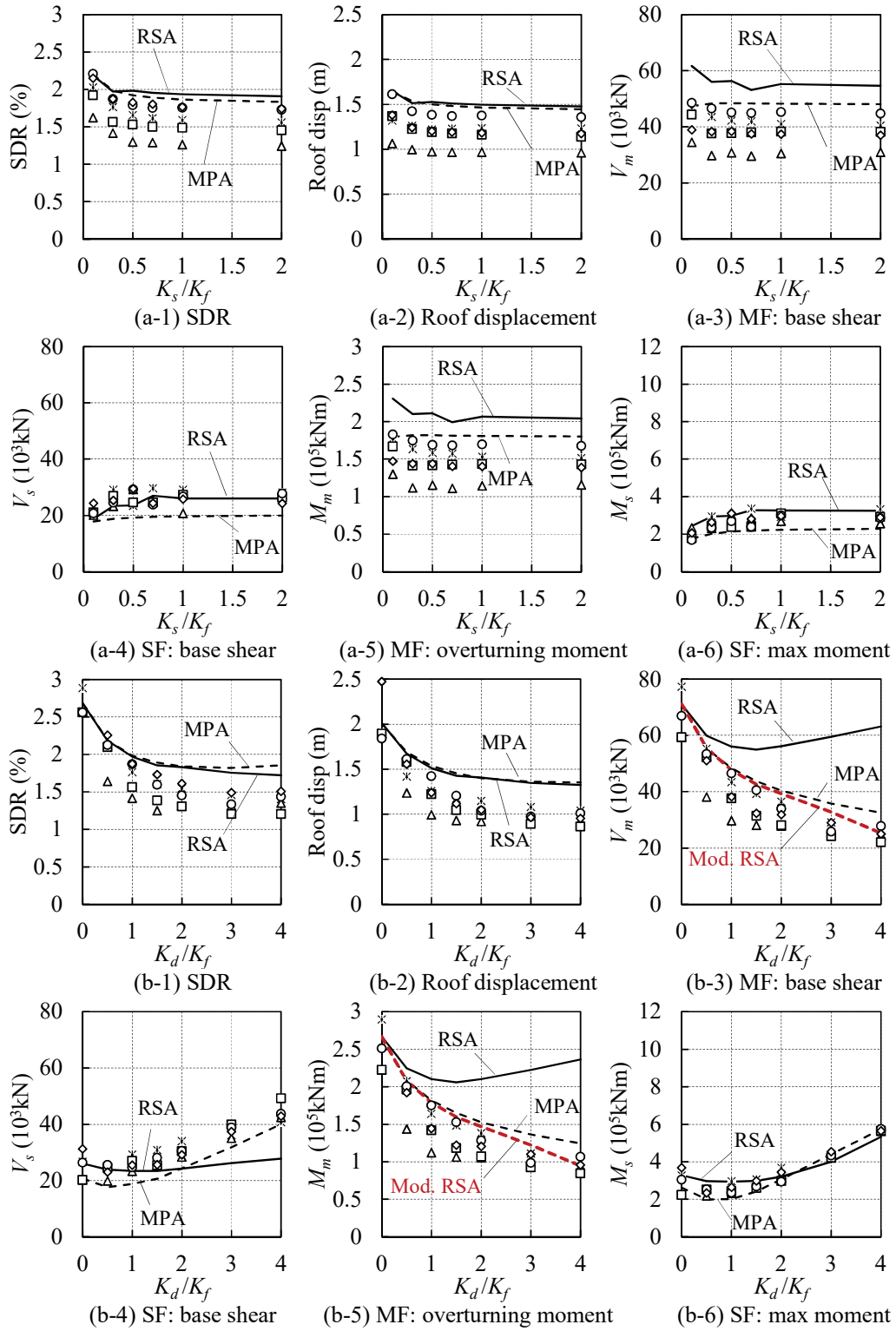

Figure 24. Comparison of RSA, MPA, and THA on seismic response of Sgt2 models: (a) with various K_s/K_f(K_d/K_f=1.0); (b) with various K_d/K_f(K_s/K_f=0.3)

CONCLUSIONS

In this study, the seismic performance of high-rise buildings adopting controlled spine frame structures was studied and a segmented-spine frame configuration was proposed. Seismic evaluation methods based on modal pushover analysis and response spectrum analyses have been developed for high-rise buildings adopting continuous or segmented spine frames. A parametric study was conducted to examine the optimal ranges for key structural parameters and to verify the proposed evaluation methods. The following conclusions were drawn from this study:

(1) The stiff spine frame has an effect in achieving a more uniform deformation distribution, even for structures as tall as 30 stories. To ensure the effectiveness of the spine frame and dampers, the spine-to-moment frame stiffness ratio K_s/K_f should exceed 0.3 for buildings higher than 10 stories. Increasing the damper stiffness is not always effective to reduce the seismic performance of the buildings. It is recommended to set the damper-to-moment frame stiffness ratio K_d/K_f up to 2.0 for the typical case of $0.3 \leq K_s/K_f \leq 2.0$.

(2) For buildings higher than 20 stories, as long as segment location $N_{b1}/N = 0.5–0.75$ and upper-to-lower damper stiffness ratio $K_{d2}/K_{d1} \geq 0.5$, the 2-segment spine frame model could ensure a similar SDR response and efficiently reduce the base shear, compared to the continuous single-spine frame model. Therefore, the 2-segment spine frame configuration is recommended for high-rise buildings when the number of BRCs at one story is limited. The 3-segment spine frame model cannot achieve better performance than the 2-segment spine frame models, and its use is not recommended for buildings lower than 30 stories.

(3) The proposed MPA and RSA evaluation procedures could provide a good estimation with appropriate conservatism on the maximum deformation of continuous and segmented spine frame structures when $K_s/K_f \leq 2.0$ and $K_{d1}/K_f \leq 2.0$. The modal analysis also helps to build a deeper understanding on the dynamic response of the controlled spine frame system. The force of the moment frames, estimated by the MPA procedure, agrees well with the THA results despite of damper stiffness, i.e., number of dampers. However, the MPA method tends to underestimate the force of the spine frame. The RSA method improves the results compared to the MPA method, particularly for the maximum bending moment of the spine frame, but an additional modification factor is necessary for estimating the force of the moment frames.

ACKNOWLEDGEMENT

This research was supported by JSPS KAKENHI, Grant number 16J04449.

ABBREVIATIONS

SDR:	Story drift ratio
Cnt:	Continuous spine frame system
Sgt:	Segmented spine frame system
Prt:	Partial spine frame system
SW:	Shear wall system

REFERENCES

T. Paulay and M.J.N Priestley: Seismic design of reinforced concrete and masonry buildings, John Wiley & Sons, Inc: New York. (1992)500-516.

H. Akiyama and M. Takahashi: Ds-value for damage-dispersing type multi-story frames, J. of Struct. Constr. Engen., AIJ, 341(1984)54-61. (in Japanese)

G. A. MacRae, Y. Kimura, C. Roeder: Effect of column stiffness on braced frame seismic behavior, J. Struct. Engen. ASCE, 130.3(2004)381-391.

B. Alavi and H. Krawinkler: Strengthening of moment-resisting frame structures against near-fault ground motion effects, Earthquake Engin. Struct. Dyn. 33(2004)707-722, http://doi.org/10.1002/eqe.370.

A. Tanimura and S. Ishida: Nonlinear dynamic behavior of a Shinbashira – frame system, J. Struct. Engen. AIJ, 42.B(1996)635-642. (in Japanese)

Z. Qu, A. Wada, S. Motoyui, H. Sakata, S. Kishiki: Pin-supported walls for enhancing the seismic performance of building structures, Earthquake Engen. Dyn. 41(2012)2075-2091.

B. Janhunen, S. Tipping, J. Wolfe: Seismic retrofit of a 1960s steel moment-frame high-rise using a pivoting spine, Annual Convention of the Structural Engineers Association of California, (2013)320-336

M. Eatherton, J. Hajjar, X. Ma, H. Krawinkler, G. Deierlein: Seismic design and behavior of steel frames with controlled rocking—part I: concepts and quasi-static subassembly testing, The 2010 NASCC & Structures Congress, Orlando, USA, (2010)1523-1533.

M. Eatherton X. Ma, H. Krawinkler, D. Mar, S. Billington, J. Hajjar, G. Deierlein: Design concepts for

controlled rocking of self-centering steel-braced frames, J. Struct. Engen. ASCE, 140.11(2014).

G. MacRae, C. Clifton: Rocking structure design considerations, Steel Innovations 2013 Workshop, Steel Construction New Zealand (2013)

G.S. Djojo, G.C. Clifton, R.S. Henry: Rocking steel shear walls with energy dissipation devices, 2014 NZSEE Conference (2014)

J. Lai, S. Mahin: Strongback system: A way to reduce damage concentration in steel-braced frames, J. Struct. Engen. ASCE, 141.9(2014)

T. Takeuchi, X. Chen, R. Matsui: Seismic performance of controlled spine frames with energy-dissipating members, J. Constr. Steel Res. 114(2015)51-65, http:// doi.org/10.1016/j.jcsr.2015.07.002.

X. Chen, T. Takeuchi, R. Matsui: Simplified design procedure for controlled spine frames with energy-dissipating members, J. Constr. Steel Res. 135(2017)242-252, http://dx.doi.org/10.1016/j.jcsr.2017.04.017.

Open system for earthquake engineering simulation (OpenSees) version 2.5.0. Sponsored by Pacific Earthquake Engineering Research Center (PEER), University of California, Berkeley. Available from: http://opensees.berkeley.edu (last accessed May 2017).

H. Krawinkler and G.D.P.K. Seneviratna: Pros and cons of a pushover analysis of seismic performance evaluation. Engen. Struct. 20.4-6(1998)452-464.

A.K. Chopra, R. K. Goel: A modal pushover analysis procedure for estimating seismic demands for buildings. Earthquake Engen. Struct. Dyn. 31(2002)561-582, http://doi.org/ 10.1002/eqe.144.

A.K. Chopra, R.K. Goel, C. Chintanapakdee: Evaluation of a modified MPA procedure assuming higher modes as elastic to estimate seismic demands. Earthquake Spectra 20.3(2004)757-778, http://doi.org/10.1193/1.1775237.

R.K. Goel and A.K. Chopra: Role of higher-“mode” pushover analysis in seismic analysis of buildings. Earthquake Spectra 21.4(2005)1027-1041, http://doi.org/10.1193/1.2085189.

APPENDIX A – FORCE-DEFORMATION CURVES OF THE SDOF SYSTEM EVALUATED BY ADOPTING MPA AND RSA

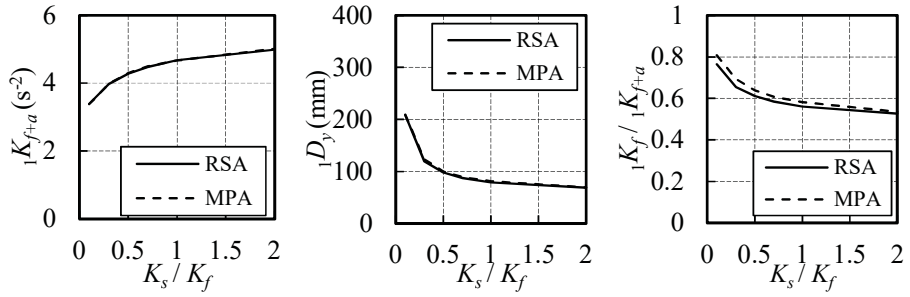

(a-1) Initial stiffness (a-2) Yielding deformation (a-3) Hardening stiffness ratio

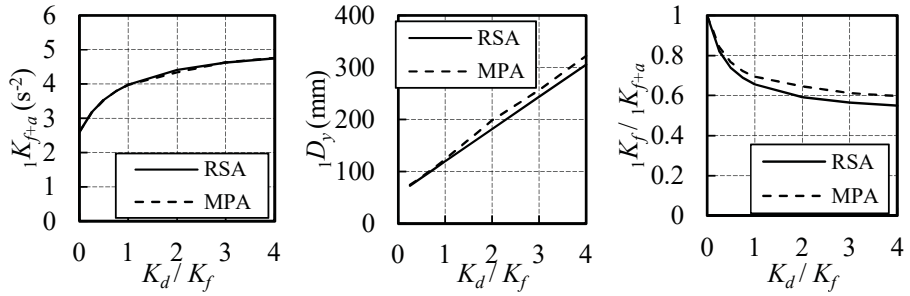

(b-1) Initial stiffness (b-2) Yielding deformation (b-3) Hardening stiffness ratio

Figure A.1 Structural characteristics of the first-mode SDOF system of Cnt models obtained by MPA and RSA methods: (a) K_d/K_f=1.0 (b) K_s/K_f=0.3

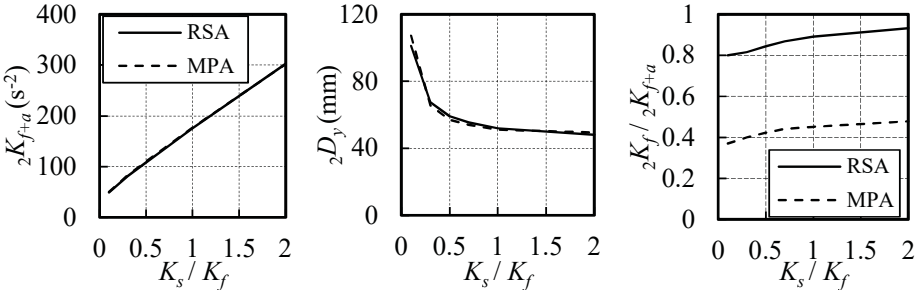

(a-1) Initial stiffness (a-2) Yielding deformation (a-3) Hardening stiffness ratio

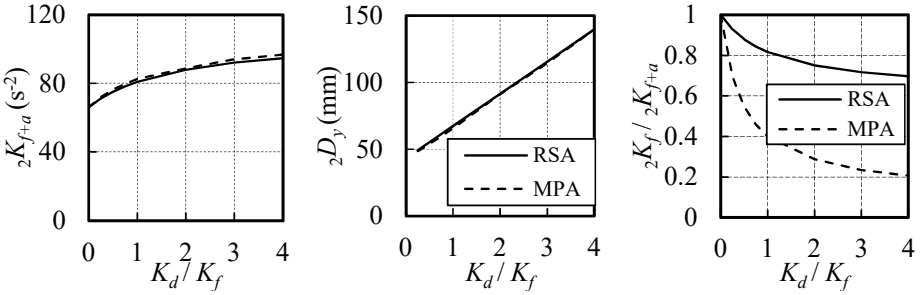

(b-1) Initial stiffness (b-2) Yielding deformation (b-3) Hardening stiffness ratio

Figure A.2 Structural characteristics of the second-mode SDOF system of Cnt model obtained by MPA and RSA methods: (a) K_d/K_f=1.0 (b) K_s/K_f=0.3

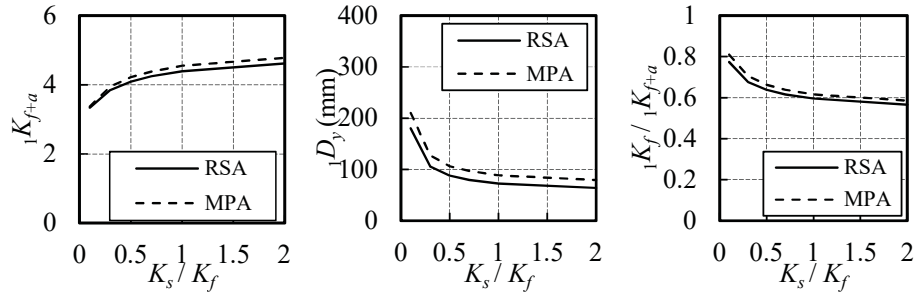

(a-1) Initial stiffness (a-2) Yielding deformation (a-3) Hardening stiffness ratio

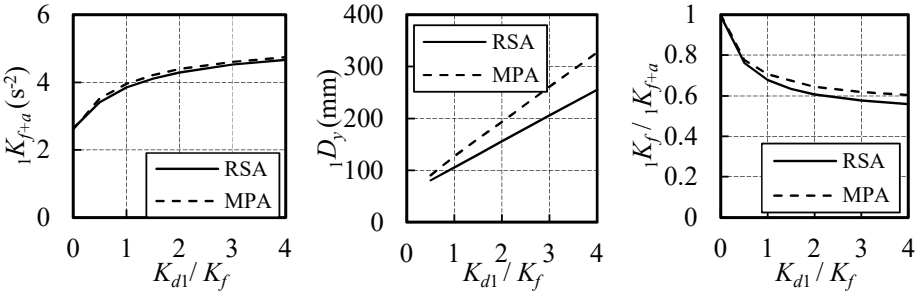

(b-1) Initial stiffness (b-2) Yielding deformation (b-3) Hardening stiffness ratio

Figure A.3 Structural characteristics of the first-mode SDOF system of Sgt2 model obtained by MPA and RSA methods: (a) K_d/K_f=1.0 (b) K_s/K_f=0.3

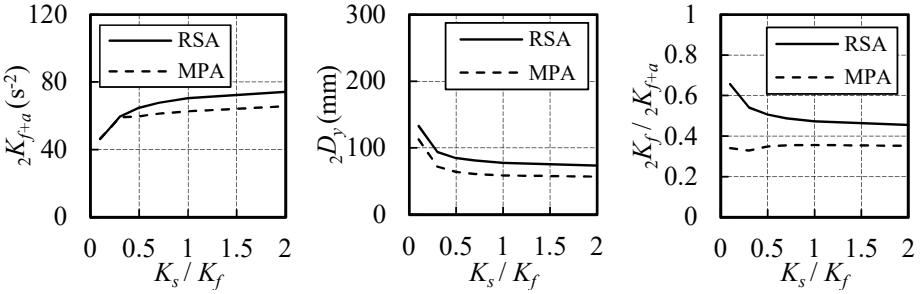

(a-1) Initial stiffness (a-2) Yielding deformation (a-3) Hardening stiffness ratio

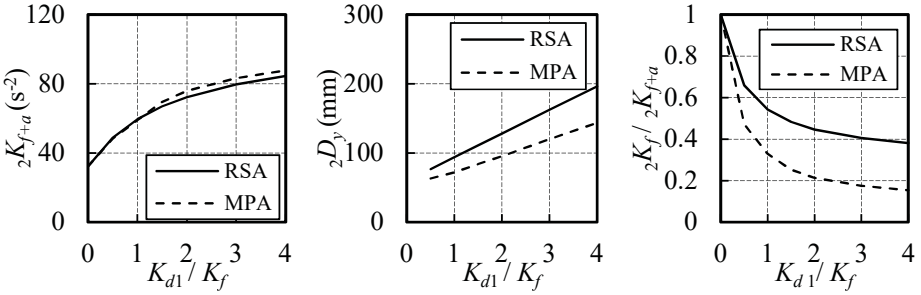

(b-1) Initial stiffness (b-2) Yielding deformation (b-3) Hardening stiffness ratio

Figure A.4 Structural characteristics of the second-mode SDOF system of Sgt2 model obtained by MPA and RSA methods: (a) K_d/K_f=1.0 (b) K_s/K_f=0.3

APPENDIX B – YIELDING MECHANISM OF DAMPERS IN THE SGT2 MODELS

The structural characteristics of the Cnt and Sgt2 models are compared by adopting the MPA method. Pushover analyses conducted on the Sgt2 models showed that the BRC2s (BRCs at the upper story) remained elastic in the first mode response. Therefore, the force-deformation curve of the first mode SDOF system of the Sgt2 models is almost identical with that of the Cnt model (Fig. B(a)). This causes that the first-mode dominant responses, such as the SDR of the Sgt2 models estimated by MPA, are almost identical with those of the Cnt models. The MPA method cannot capture the deformation reduction effect of the Sgt2 models, but still, it provides a conservative estimation on deformation and exhibits the discrepancy in forces of the Sgt2 and Cnt models.

In the second-mode pushover analysis, the BRC2s yielded first and they were followed by the BRC1s (BRCs at the first story). Yielding of the BRC2s causes less degradation in the system stiffness, while yielding of BRC1s reduces the system stiffness by approximately 50% (Fig. B(b)). The second mode SDOF system of the Sgt2 models is obviously softer than that of the Cnt models.

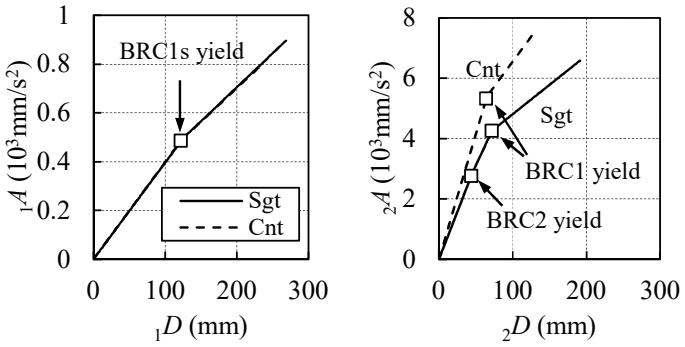

(a) First mode SDOF model (b) Second mode SDOF model

Figure B. Comparison between Cnt and Sgt2 models in SDOF A-D curves obtained by MPA (models: 20-story Cnt-Ksf0.3-Kdf1.0 and Sgt2-Ksf0.3-Nb10-Kdf1.0-0.5, input: BCJ-L2)